Research Article

Nano Research
2020, 13(3): 832–842

ISSN 1998-0124 CN 11-5974/O4
https://doi.org/10.1007/s12274-020-2704-1

Ternary Pt/Re/SnO_2/C catalyst for EOR: Electrocatalytic activity and durability enhancement

Elżbieta Drzymała[1] (✉), Grzegorz Gruzeł[1], Joanna Depciuch[1], Miroslawa Pawlyta[2], Mikołaj Donten[3], and Magdalena Parlinska-Wojtan[1]

[1] *Institute of Nuclear Physics Polish Academy of Sciences, PL-31342 Krakow, Poland*
[2] *Institute of Engineering Materials and Biomaterials, Silesian University of Technology, Gliwice 44-100, Poland*
[3] *Faculty of Chemistry, University of Warsaw, Warsaw 02-093, Poland*

Received: 18 November 2019 / **Revised:** 17 January 2020 / **Accepted:** 8 February 2020

ABSTRACT

Carbon-supported Pt/C, Pt/Re/C, Pt/SnO_2/C and Pt/Re/SnO_2/C, with 20 wt.% overall metal loading were prepared and their electrochemical activity towards ethanol oxidation reaction (EOR) was investigated. Transmission electron microscopy (TEM) combined with energy dispersive X-ray spectroscopy (EDS) revealed, that indeed binary and ternary combinations of the designed nanoparticles (NPs) were formed and successfully uniformly deposited on a carbon support. Fourier transform infrared spectroscopy (FTIR) allowed to assess the chemical composition of the nanocatalysts and X-ray diffraction (XRD) allowed to determine the catalyst structure. Potentiodynamic and chronoamperometric measurements were used to establish its catalytic activity and stability. The influence of Re addition on the electrochemical activity towards ethanol oxidation reaction (EOR) was verified. Indeed, the addition of Re to the binary Pt/SnO_2/C catalyst leads to the formation of ternary Pt/Re/SnO_2/C with physical contact between the individual NPs, enhancing the EOR. Furthermore, the onset potential of the synthesized ternary catalyst is shifted to more negative potentials and the current densities and specific activity are nearly 11 and 5 times higher, respectively, than for commercial Pt catalyst. Additionally ternary Pt/Re/SnO_2/C catalyst retained 96% of its electrochemical surface area.

KEYWORDS

chemical synthesis, transmission electron microscopy (TEM) characterization, electrochemistry, ethanol oxidation reaction (EOR), Pt/Re/SnO_2/C catalysts, ternary catalysts

1 Introduction

A lot of current research on fuel cell technology is often based on the use of liquid fuel—methanol and ethanol [1–4]. It is interesting due to the simplicity of usage, transport and storage. Additionally ethanol is non-toxic, can be obtained from biomass and opens the possibility of replacing toxic methanol [5, 6]. However, the usage of ethanol as a fuel creates various challenges, such as the difficulty to split the C–C bond or slow kinetics of the ethanol oxidation at the anode and thus requires optimization of the catalysts. Moreover, during the ethanol oxidation reaction (EOR) it is possible to form unwanted by-products, which may reduce the total efficiency [7, 8]. The complete oxidation of ethanol is dependent on many factors like ethanol concentration, temperature or composition and structure of the catalyst used. Therefore one of the main goals is to design and develop the appropriate type of catalysts, because the success of fuel cells will largely depend on improving their performance. Because catalysis is a surface effect, the catalyst needs to have the largest possible surface area [9] and that is why researchers study, apart from the chemical composition, the effect of size for both, platinum [10] and tin oxide [11] nanoparticles (NPs), in alcohol oxidation reactions.

Carbon supported nanostructured platinum is commonly used as an electrocatalyst for ethanol oxidation, but is not the optimal anodic catalyst for direct ethanol fuel cells (DEFCs) [1]. This is associated with the intermediate species e.g. CH_x and CO formed during the electrooxidation of ethanol, which poison active sites on the Pt surface, because of their strong interaction with Pt [7]. Moreover, Pt has limited ability for breaking the C–C bond [12]. For this reason studies to develop and obtain highly active EOR electrocatalysts are concentrated on the addition of co-catalysts to platinum and preparation of multi-component and multifunctional nanostructured particles. The presence of oxophilic metals/component, such as Ru, Sn or SnO_2 activate water dissociation to form surface hydroxides, which can more readily oxidize CO and CH_x intermediates, free Pt active sites and therefore promote CO electrooxidation [13, 14].

It is known that binary PtSn catalysts have a high EOR activity—Antolini [15, 16] reviewed the most relevant research and widely analyzed the promoting effect of Sn on the activity of Pt catalysts. Li et al. [17] highlighted also, that both too high and too low Sn contents, cause a decrease in the catalyst's activity. But it is worth noticing, that binary nanoparticles containing Pt and Sn are active electrocatalysts for the EOR, but inactive for splitting the C–C bond of ethanol to form CO_2 [18, 19]. That is why scientists state that the activity towards ethanol oxidation not only depends on the ability of the catalyst for oxidative removal of poisoning species, but also on its activity for C–C and C–H bond breaking [19]. Oxidizing

Address correspondence to elzbieta.drzymala@ifj.edu.pl

ethanol to CO_2 and water is not easy, because the C–C bond requires a rather high activation energy [19], and in order to modify the characteristics of the two-component catalysts and improve their performance it is necessary to insert a third element. The Adzic group tested Rh or Ir as this third element [17, 20, 21]. Kowal et al. [22] prepared a PtRh/SnO_2/C electrocatalyst by synthesizing Pt and Rh atoms on carbon-supported SnO_2 nanoparticles and reported that the ternary PtRh/SnO_2/C catalyst was effective for ethanol oxidation to CO_2 by synergetic effect between Pt, Rh and SnO_2. They also showed, using density functional theory calculations, that the addition of Rh to the Pt-SnO_2 catalyst promotes breaking of the C–C bond. In their case Pt and Rh formed an alloy, while the Higuchi group [23] studied the catalyst of the same composition for EOR and showed that the current density for CO_2 production of the Rh-containing catalysts was smaller than that of the Pt/SnO_2/CB catalyst, in contrast to what the Kowal showed [22]. However, this discrepancy may be caused by the fact, that the Pt, Rh and SnO_2 nanoparticles prepared by Higuchi et al. [23] were only partially contact with each other, which was confirmed using TEM images, while Kowal et al. prepared the PtRh NPs in form of a nanoalloy.

In the present study, rhenium as the third element in addition to Pt and SnO_2 was selected. Literature reports indicate that Re addition to Pt-based catalysts supported on metal oxides similarly to Rh increases the ability to break the C–C bond [24–26]. Higher activity for Pt-Re was also attributed to the weakening of Pt–CO binding strength with the addition of Re and decreased poisoning of active surface sites by adsorbed CO [25, 27, 28]. Pt and Re differ in crystallographic structure. Re has a hexagonal (hex) space group $P6_3/mmc$ with lattice constants of 2.760 and 4.456 Å, while Pt belongs to a face-centered cubic (fcc) having the $Fm3m$ space group with a lattice constant equal to 3.920 Å [29]. Therefore, obtaining a PtRe alloy may be more difficult than obtaining a PtRh alloy, and may thus require complicated synthesis procedures in comparison with the formation of the PtRh alloy. This is due to the fact, that rhodium has the same space group and very similar lattice constants to Pt [30]. These facts favor the formation of a homogeneous binary PtRh alloy, in particular the PtRe alloys are often synthesized in form of films [28, 31, 32]. In the present study Re nanoparticles were synthesized separately and combined with platinum and tin oxide NPs. In a previous study [33] it has been shown that by adjusting the zeta potential of the respective nanoparticles it was possible to obtain in a controlled way SnO_2 nanoparticles decorated with platinum or rhenium nanoparticles or both of them. The idea of close contact between the respective NPs, proposed by Higuchi et al. will be thus verified by replacing Rh with Re. Roth et al. also indicated that alloy formation does not seem to be fundamental for superior electrocatalytic performance, as long as a close contact between both phases is achieved [34]. The electrocatalytic surfaces studied here show an interesting approach for the investigation of non-alloy systems with close contact between three nanoparticle phases.

In the present paper, a ternary nanocatalyst system consisting of Pt, Re and SnO_2 nanoparticles was prepared and characterized using high resolution transmission electron microscopy (HR-TEM) with energy dispersive X-ray spectroscopy (EDS), Fourier transform infrared spectroscopy (FTIR) and X-ray diffraction (XRD). In the case of ternary catalysts, understanding the role of each constituent is needed for obtaining a high electrocatalytic activity. In this work, special attention has been focused on investigating the role of Re in the ternary system, as an alternative to Rh, as well as the physical contact between three components building nanocatalyst. Furthermore, cyclic voltammetry (CV) and chronoamperometry (CA) experiments were carried out, to study the electrocatalytic activity on ethanol electrooxidation and additionally allowed to investigate the durability of the synthesized catalysts.

2 Experimental

2.1 Materials

Hexachloroplatinic acid hydrate ($H_2PtCl_6{\cdot}6H_2O$), tin(II) chloride dihydrate ($SnCl_2{\cdot}2H_2O$) from Sigma Aldrich and ammonium perrhenate (NH_4ReO_4) from Alfa Aesar were used as metal sources. Ethylene glycol (EG, $C_2H_6O_2$), sodium borohydride ($NaBH_4$), ethanol (C_2H_5OH), propanol (C_3H_7OH) and sodium hydroxide (NaOH) were obtained from Avantor. Polyvinyl-pyrrolidone (PVP) was purchased from Sigma Aldrich. Nafion solution 5‰ (Aldrich) and high surface area carbon Vulcan XC-72R (Cabot) were used as received.

2.2 Synthesis methods

Carbon-supported Pt/C, Pt/Re/C, Pt/SnO_2/C, and Pt/Re/SnO_2/C, with 20 wt.% overall metal loading were prepared using a modified polyol method. In the first step monometallic Pt, Re and SnO_2 nanoparticles were prepared using the same procedure as in Drzymała et al. [33]. In brief, the calculated amount of H_2PtCl_6 (Sigma Aldrich) was dissolved in ethylene glycol. Next, this solution was placed in a round-bottom flask and the pH of the solution was subsequently adjusted to 12 using a 0.5 M NaOH solution diluted in EG. Then the obtained solution has been heated to reflux for 3 h and cooled down overnight. The SnO_2 NPs were synthesized from $SnCl_2{\cdot}2H_2O$ (Sigma Aldrich) dissolved in a solution containing water and EG (with a molar ratio $[H_2O]/[EG] = 0.02$). In the next step, similar to Pt NPs, the pH of the solution was subsequently adjusted to 12 and heated to reflux for 6 h. Finally both types of the obtained nanoparticles were centrifuged and washed with ethanol and distilled water. Prior to addition, the carbon support (Vulcan XC-72R, Cabot) was heated at 100 °C for 1 h under a pure nitrogen atmosphere and was oxidized by contact with a solution of HNO_3 and H_2O in order to form surface functional groups (hydroxyl and carboxylic acid), which could be further used to disperse the metal by exchanging protons with metal complexes. As a precursor for the synthesis of rhenium nanoparticles ammonium perrhenate NH_4ReO_4 (Alfa Aesar) was used. The reaction was carried out under argon atmosphere. The Re NPs were synthesized according to the procedure described in previous works [33, 35]. These nanoparticles were added separately to the mixture of Pt and SnO_2 NPs. Adjusting the zeta potential values to opposite signs for the NPs allowed to successfully assembly the three component combination by mixing the solutions containing the NPs synthesized according to our previous work [33].

In the last step of catalyst preparation, high surface area carbon black was dispersed in a water and ethanol solution and sonicated for 30 min. Simultaneously, the re-dispersed nanoparticles also were sonicated. Next the re-dispersed nanoparticles and their combinations were deposited on a calculated amount of Vulcan XC-72R carbon support (being introduced drop-wise under vigorous stirring), and the mixture was mixed overnight under magnetic stirring. The resulting black powder was then washed with ethanol and distilled water and was dried at 80 °C overnight (10 h). Finally, the catalysts were annealed at 200 °C for 1 h to remove remaining ethylene glycol.

2.3 Experimental techniques

2.3.1 TEM measurements

High-angle annular dark field scanning TEM (HAADF-STEM) and selected-area electron diffraction (SAED) were performed using a Cs aberration-corrected FEI Titan electron microscope operating at 300 kV equipped with a FEG cathode. EDS studies were carried out in a Talos F200 FEI instrument operating at 200 kV equipped with a FEG cathode. The TEM samples were prepared by placing a drop of electrocatalyst dispersed in ethanol onto a continuous carbon foil coated copper grid.

2.3.2 XRD

The XRD studies were carried out using the X'Pert PRO (Panalytical) diffractometer with Cu Kα (1.5404 Å) radiation, a graphite monochromator and a strip detector (X'Celerator). To preclude any extra diffraction lines, the samples were placed onto a "zero-background" silicon plate. The experiments were performed at room temperature. The XRD patterns were vector normalized and base line correction was applied using the OriginPro 8.0 software.

2.3.3 FTIR spectroscopy

The FTIR spectra in the wavelength range between 400–4,000 cm^{-1} were acquired using an EXCALIBUR FTS-3000 spectrometer at room temperature and measured for the respective samples mixed with KBr. The sample was dried and sandwiched between two KRS-5 window disks. The 64 scans were averaged at a resolution of 4 cm^{-1}. During the experiments, the spectrometer was purged with dry nitrogen. Baseline correction and normalization of FTIR spectra were applied.

2.3.4 Inductively coupled plasma mass spectrometry (ICP-MS)

ICP-MS measurements were carried out on a Perkin Elmer NexION 300D in order to prepare catalysts with 20% Pt loading. The sample preparation procedure was as follows: First the sample solution was intensively mixed and sonicated for 15 min and next 0.5 mL of the solution was collected and evaporated at 50 °C. In the next step, 2 mL of aqua regia was added to the flask containing the nanoparticles and heated close to the boiling point until the precipitate was dissolved. After that the solution was evaporated to a volume of 0.5 mL and the sample was ready for ICP-MS measurement.

2.3.5 Electrochemical measurements

A BIO-LOGIC SP-200 potentiostat was used for the electrochemical measurements in a standard three-electrode electrochemical cell. Uniform catalyst inks were prepared by ultrasonically mixing 4 mg of catalysts powder with 800 μL of isopropyl alcohol, 200 μL of ultrapure water, and 20 μL of 5 wt.% Nafion solution for 30 min. Then 10 μL of ink suspension was deposited onto a polished glassy carbon electrode (GCE) to obtain the working electrode with a homogenous thin catalyst layer, after the solvent dried naturally in air. Both CV and CA measurements in ethanol-containing solution were carried out to determine the EOR activity of these catalysts. The glassy carbon electrode loading was 40 μg/cm^2 (platinum loading). A standard glass cell with a Pt counter electrode and a silver chloride reference electrode was used. The electrolyte, containing 0.1 M $HClO_4$ and 0.5 M C_2H_5OH, was deoxygenated by bubbling Ar for 30 min before measurements. All the potentials given in this paper were referenced to that of the reversible hydrogen electrode (RHE). The commercial Pt TANAKA with 40 wt.% metal loading was also tested as a reference. All measurements were performed at room temperature.

Additionally, accelerated stability tests of the synthesized nanocatalysts and the commercial Pt TANAKA were performed by consecutive sweeps from 0 to 1.2 V vs. RHE at 100 mV/s for 10,000 potential cycles in a 0.1 M $HClO_4$ solution.

3 Results

3.1 TEM analysis

Tin oxide, platinum and rhenium nanoparticles as well their combinations were synthesized and characterized in details in previous work [33, 35]. Briefly, in all cases crystalline, small (bellow 10 nm) spherical nanoparticles were obtained. The diameters of tin, platinum and rhenium nanoparticles assembled into binary and ternary catalysts were 4.6 ± 0.7, 2.0 ± 0.3 and 1.0 ± 0.2 nm, respectively (Fig. S1 in the Electronic Supplementary Material (ESM)). Next, based on the differences in zeta potential and due to the electrostatic interactions, binary metal-metal and metal-oxides nanoparticle systems were successfully assembled (Figs. 1(b) and 1(c)).

Binary Pt/SnO_2 and ternary Pt/Re/SnO_2 nanoparticle systems were assembled as described in detail in a previous study [33]. The obtained Pt NPs, binary and ternary combinations were deposited on high-surface area carbon (Vulcan XC-72R) (Figs. S2 and S3 in the ESM). The HAADF-STEM image of Pt/Re/SnO_2/C (Fig. 2(a)) shows that the nanoparticles were uniformly dispersed on the carbon surface, with no visible agglomerates. Nanoparticles have a crystalline structure, which is confirmed by both the SAED pattern (Fig. 2(b)) and the high resolution HAADF-STEM image (Fig. 2(c)). Moreover, the high resolution HAADF-STEM image (Fig. 2(c)) shows that all three kinds of nanoparticles are well-mixed and stay in physical contact. Pt, Re and SnO_2 NPs can be distinguished due to different *Z*-numbers and thereby different contrasts on the HAADF-STEM images (so-called *Z*-contrast). Additionally, in Fig. 2(c) the differences in lattice parameters are visible. The measured lattice distances between the atomic planes marked in red correspond to (111) planes of fcc Pt, in yellow to (101) and (102) planes of hcp Re and in blue to (101) and (110) planes of tetragonal SnO_2. EDS

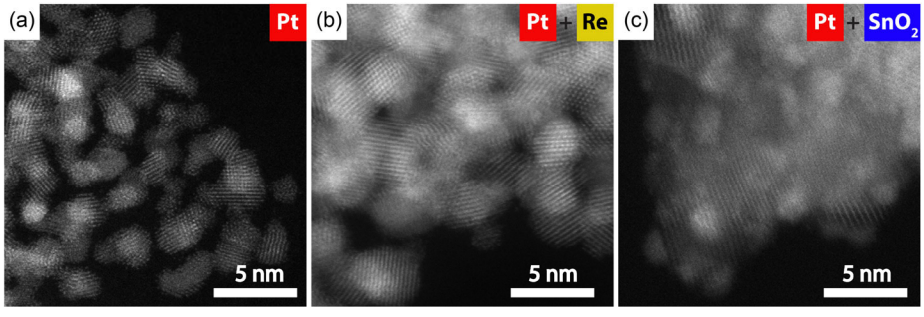

Figure 1 HAADF-STEM images of synthesized (a) Pt NPs and combinations of (b) Pt with Re NPs and (c) Pt with SnO_2 NPs.

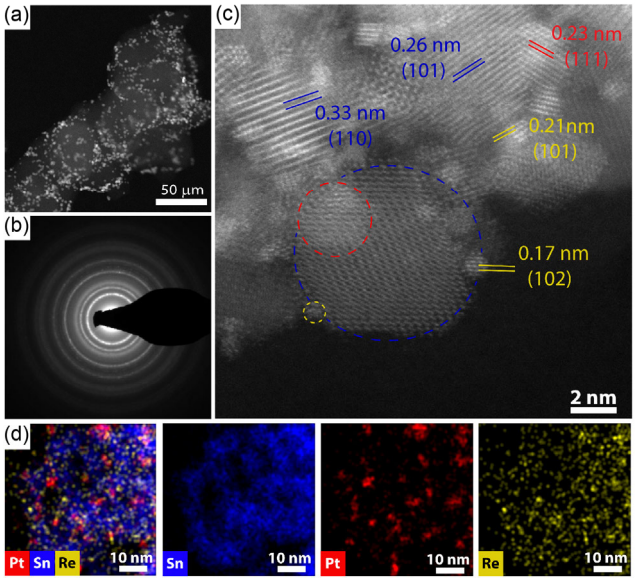

Figure 2 Pt/Re/SnO_2 nanoparticles deposited on Vulcan carbon XC-72R: (a) HAADF-STEM overview image; (b) SAED pattern; (c) high resolution HAADF-STEM image with measured lattice distances corresponding to Pt (red), Re (yellow) and SnO_2 (blue) and (d) EDS elemental maps showing the distribution of Pt, Re and SnO_2 nanoparticles.

elemental maps confirm the presence of platinum, rhenium and tin and clearly show that all elements are uniformly mixed. The distribution of nanoparticles in other obtained catalysts was also studied by TEM. All of them showed a uniform distribution of the nanoparticles supported on carbon (Figs. S2(a)–S2(d) in the ESM).

3.2 XRD analysis

Figure 3 shows the X-ray diffractograms for Pt/C, Pt/Re/C, Pt/SnO_2/C and Pt/Re/SnO_2/C catalysts. The Bragg peak positions were compared with the reference XRD diffractograms of Pt, Re and SnO_2 (PDF data files, International Center for Diffraction Data). According to literature, the broad diffraction peak at around $2\theta = 25°$ corresponds to the (002) plane of the Vulcan XC-72R carbon support [36]. In all obtained catalysts the five characteristic peaks of face centered cubic crystalline Pt located at 2θ angles of ca. 39.8°, 46.4°, 67.5°, 81.3° and 85.8° and corresponding to the (111), (200), (220), (311) and (222) planes, were observed. In the Pt/Re/C catalyst a sharp reflex located at 18.4° corresponding the (002) planes of the hcp Re was observed. Two other reflexes with low intensity from the (300) and (102) planes of the hcp Re are also visible at 2θ equal to approximately 52.7° and 56.4°, respectively. Additionally, platinum and rhenium have overlapping reflections, and as the Pt NPs are better crystalized and larger, they generate sharper reflexes and thus it is difficult to identify the diffraction peaks corresponding to rhenium. As clearly indicated from the HAADF-STEM images (Fig. 2(c)), rhenium was synthesized in form of 1 nm small, crystalline particles, therefore it would most probably invisible in XRD diffractograms. Additionally, the diffraction peak originating from rhenium oxide (black open circles) was also observed, which is consistent with the X-ray photoelectron spectroscopy (XPS) results in our previous work [33]. According the XPS measurements, tetravalent tin, proving the formation of SnO_2, metallic rhenium and metallic platinum nanoparticles were obtained. In the XRD diffractogram for the Pt/SnO_2/C and Pt/Re/SnO_2/C catalysts, SnO_2 tetragonal structure was observed. In the Pt/SnO_2/C sample four characteristic peaks of tetragonal SnO_2 located at scattering angles equal approximately to 33.8°, 51.8°, 61.9° and 74.5°

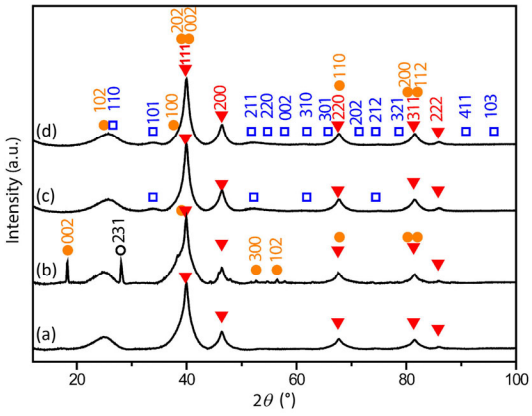

Figure 3 X-ray diffractograms of the (a) Pt/C; (b) Pt/Re/C; (c) Pt/SnO_2/C and (d) Pt/Re/SnO_2/C catalysts with the corresponding planes. In order to compare the diffractograms, the peaks were normalized to maximum intensity. The elements are marked as follows: Pt (▼), Re (●), Re_2O_7 (○), SnO_2 (□).

corresponding to the (101), (211), (310) and (212) planes, were present. In case of the Pt/Re/SnO_2/C catalyst, more reflexes originating from tin oxide are visible. Also, there were no evident peaks from metallic Sn. Additionally, the XRD diffractogram of commercially available Pt TANAKA is shown in Fig. S4 in the ESM.

3.3 FTIR spectroscopy analysis

The chemical composition of the synthesized nanoparticles was analyzed using FTIR spectroscopy. Figure 4 (solid lines) shows the FTIR spectra of the nanoparticles deposited on carbon. In the FTIR spectrum of all analyzed samples vibrations building

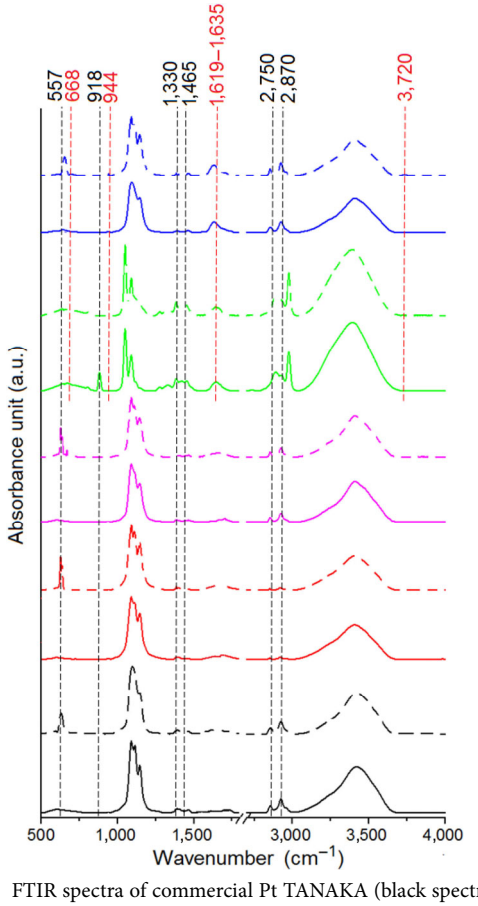

Figure 4 FTIR spectra of commercial Pt TANAKA (black spectra), Pt/C (red spectra), Pt/Re/C (pink spectra), Pt/SnO_2/C (green spectra), and Pt/Re/SnO_2/C (blue spectra) catalysts before (full line) and after (dotted line) 10,000 potential cycles.

the chemical compounds used to reduce the precursors and wash the samples, were visible: outer and interface of the OH group from PVP (wavenumbers at: 918 cm^{-1}) [37], bending vibrations of the CH_2 group from ethylene glycol (1,465 cm^{-1}), CH stretching symmetric and asymmetric vibrations (2,750 and 2,870 cm^{-1}, respectively) [38, 39]. Moreover, in all obtained FTIR spectra, a peak at 1,330 cm^{-1} corresponding to the NO_2 group from HNO_3 used for carbon functionalization, was visible. Furthermore, a peak between 1,619 and 1,635 cm^{-1} corresponding to OH vibrations from H_2O originating from H_2O absorbed on the surface of SnO_2 [40–42] or from the chemical decomposition of $HClO_4$ in the all FTIR spectra of $PtSnO_2$/C and Pt/Re/SnO_2/C was noticed [43, 44]. Additionally, FTIR was used to track the vibrational peaks and changes of the individual nanoparticles in the catalysts after 10,000 potential cycles (Fig. 4, dotted line). Comparing the FTIR spectra of Pt TANAKA, Pt/C, Pt/Re/C, Pt/SnO_2/C, Pt/Re/SnO_2/C catalysts before and after 10,000 potential cycles, the vibration from $HClO_4$, in the spectra after cycling, was observed [44]. Moreover, after 10,000 potential cycles in the FTIR spectra of Pt/SnO_2/C and Pt/Re/SnO_2/C, the stretching vibrations of O–Sn–O from SnO_2, were absent. Furthermore, the catalytic reaction caused the appearance of a peak at 3,720 cm^{-1} in the FTIR spectrum of Pt/Re/SnO_2/C. All peaks presented in Fig. 4 are summarized in Table 1.

3.4 Ethanol electrooxidation/electrochemical characterization

All catalysts were prepared with the same platinum metal loading (20 wt.%), which was evaluated by ICP-MS. The catalyst powders were suspended in water, isopropyl alcohol and 5‰ Nafion solution and applied onto a glassy carbon electrode. After having immersed the electrode in the supporting electrolyte, the potential was cycled between 0 and 1 V (vs. RHE) for all catalysts in order to prevent dissolution of Sn.

The electrochemical activity of carbon supported catalysts Pt/C, Pt/Re/C, Pt/SnO_2/C and Pt/Re/SnO_2/C compared to commercial Pt TANAKA was verified by CV, and their performance towards EOR was investigated. Results for Re/C and Re/SnO_2/C were not presented in the paper because the obtained curves did not contain the characteristic hydrogen adsorption/desorption region, based on which the electrochemically active surface is calculated. As a consequence of the absence of Pt in both systems, ethanol adsorption probably did not occur on the surface of the catalysts. Figure 5 shows the cyclic voltammograms for the catalysts measured in 0.1 M $HClO_4$, at a scan rate of 50 mV/s without ethanol, in a standard three-electrode electrochemical cell, from which the hydrogen absorption region was used to calculate the electrochemically active surface area (ECSA; Table 2). The contribution from the double layer current was removed. The procedure of calculation of the ECSA value is shown in Fig. S5 in the ESM. The scan was repeated several times to ensure that stable CV curves were obtained. The profiles presented in Fig. 5 correspond to the second cycle of the respective catalysts. The first potential region from ~ 0 to 0.3 V vs. RHE corresponds to the adsorption/desorption of hydrogen. The CVs curves for the Pt TANAKA, Pt/C and Pt/Re/C have a very similar course and all the catalysts show a characteristic well-defined hydrogen adsorption–desorption region as usually observed for Pt catalyst [5, 45–47]. The cyclic voltammograms of the Pt/SnO_2/C and Pt/Re/SnO_2/C catalysts additionally showed an increase in current density at the double layer and two characteristic peaks at about 0.45 and 0.7 V, which is related to the presence of Sn oxide species [5, 46, 48, 49]. The ECSAs of Pt TANAKA, Pt/C, Pt/Re/C, Pt/SnO_2/C and Pt/Re/SnO_2/C catalysts were 169.8, 285.9, 349.0, 125.5 and 56.95 cm^2/mg_{Pt}, respectively.

In the next step in order to evaluate the electrocatalytic activity for ethanol oxidation, C_2H_5OH was added into the electrolyte and after 30 min argon-purging the solution, the experiment was continued. Figure 6(a) shows the cyclic voltammograms of ethanol oxidation under acidic conditions (0.5 M C_2H_5OH and 0.1 M $HClO_4$) for the all synthesized catalysts in comparison with commercial platinum. The values of current were normalized by the ECSA and the mass loading of Pt, considering that ethanol adsorption occurs only on the Pt sites [46].

The Pt/Re/SnO_2/C shows a specific activity of 0.43 mA/cm^2 at 0.45 vs. RHE, which is near 5 times higher than that of the commercial Pt TANAKA catalyst (0.09 mA/cm^2) (Fig. 7(b)). For the other binary catalysts, the specific activity is also lower than that for the ternary catalyst.

The Pt/Re/SnO_2/C catalyst shows significantly higher activity for ethanol oxidation than the others. The area and mass normalized current density at 0.45 V for the Pt/Re/SnO_2/C catalyst is about 11-fold that of the commercial Pt catalyst. Moreover, the current densities of ethanol oxidation on the Pt/Re/SnO_2/C catalyst sharply increase in the region around

Table 1 FTIR analysis of the studied nanoparticles. X means that the vibration is not present in the FTIR spectrum of catalysts; B—before and A—after 10,000 potential cycles

Wavenumber (cm^{-1})	Bond/ stretching functional group	Pt TANAKA		Pt/C		Pt/Re/C		Pt/SnO_2/C		Pt/Re/SnO_2/C	
		B	A	B	A	B	A	B	A	B	A
557	Vibrations from $HClO_4$	X		X		X		X		X	
668	Stretching vibrations of Sn–O–Sn from $Sn(OH)_4$	X	X	X	X	X	X				
918	OH outer face vibration from PVP										
944	Stretching vibrations of O–Sn–O from SnO_2	X	X	X	X	X	X		X		X
1,330	NO_2 stretching from HNO_3										
1,465	CH_2 bending from glycole										
1,619–1,635	OH vibrations from H_2O adsorbed on the surface of SnO_2 or the chemical decomposition of $HClO_4$	X	X	X	X	X	X	X		X	
2,750	CH stretching symetric from glycol and PVP										
2,870	CH stretching asymetric from glycol and PVP										
3,720	OH vibrations from H_2O adsorbed on the surface of $SnCl_4H_2O_2$	X	X	X	X	X	X	X	X	X	

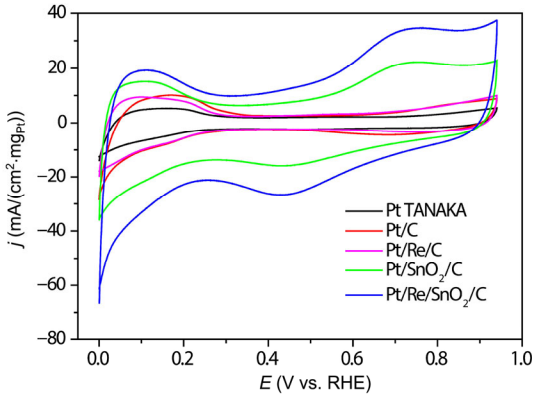

Figure 5 Cyclic voltammetry of commercial Pt TANAKA, Pt/C, Pt/Re/C, $Pt/SnO_2/C$, and $Pt/Re/SnO_2/C$ electrocatalysts in 0.1 M $HClO_4$, sweep rate (50 mV/s).

Table 2 ECSA calculated from the hydrogen adsorption/desorption region for commercial Pt TANAKA, Pt/C, Pt/Re/C, $Pt/SnO_2/C$ and $Pt/Re/SnO_2/C$ catalysts

Catalyst	Pt TANAKA	Pt/C	Pt/Re/C	Pt/SnO_2/C	Pt/Re/SnO_2/C
ECSA (cm^2)	3.26	2.28	2.79	1.00	0.45
ECSA (cm^2/mg_{Pt})	169.8	285.9	349	125.5	56.95

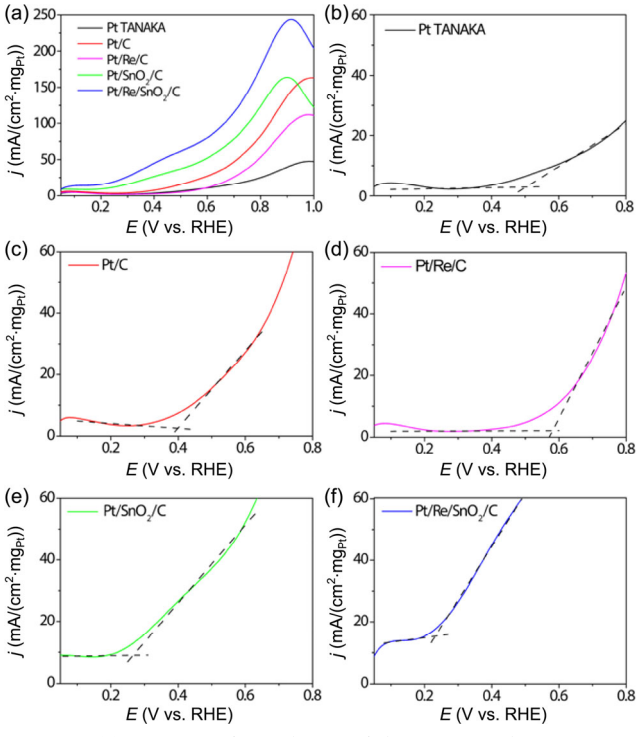

Figure 6 (a) First EOR forward scan of the commercial Pt TANAKA and synthesized catalysts with marked onset potential region for (b) Pt TANAKA; (c) Pt/C; (d) Pt/Re/C; (e) $Pt/SnO_2/C$ and (f) $Pt/Re/SnO_2/C$. All curves were recorded in 0.1 M $HClO_4$ + 0.5 M C_2H_5OH solution at a scan rate of 50 mV/s at room temperature.

0.4 V (vs. RHE), while for the commercial Pt TANAKA catalyst the current increases slightly at around 0.6 V (vs. RHE). The onset potential of ethanol oxidation is by about 0.3 V lower for the $Pt/Re/SnO_2/C$ catalysts than for the commercial Pt TANAKA, which is shown in Figs. 6(b)–6(f) and Table 3. For Pt/C and $Pt/SnO_2/C$ catalysts the value of onset potential was also shifted negatively in comparison to Pt commercial.

Additionally the Pt/C, Pt/Re/C, $Pt/SnO_2/C$ and $Pt/Re/SnO_2/C$

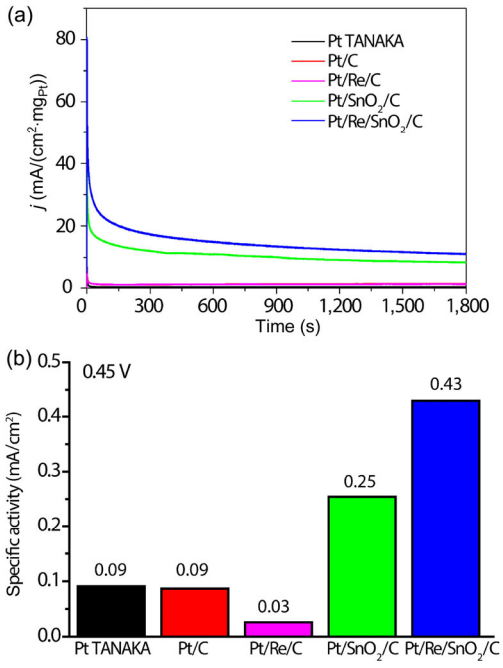

Figure 7 (a) Current–time curves recorded at 0.45 vs. RHE for 1,800 s in 0.1 M $HClO_4$ + 0.5 M ethanol solution; (b) histogram of EOR specific activity at 0.45V vs. RHE compared with commercial Pt TANAKA. Scan rate is equal to 50 mV/s at room temperature.

Table 3 Comparison of the onset potential values for all tested catalysts

Sample	Pt TANAKA	Pt/C	Pt/Re/C	Pt/SnO_2/C	Pt/Re/SnO_2/C
Onset potential vs. RHE (V)	0.51	0.40	0.58	0.27	0.23

catalysts performances towards ethanol oxidation were studied by chronoamperometry in 0.5 M of ethanol in 0.1 M $HClO_4$ at an anodic potential of 0.45 V vs. RHE (Fig. 7(a)). In all current–time curves there was an initial current drop in the first 3 min followed by a slower decay, but the current values obtained for ternary $Pt/Re/SnO_2/C$ catalysts were always higher than those obtained for the other studied catalysts and commercial Pt.

To check the durability of the obtained catalysts in acidic conditions compared to the commercial Pt TANAKA catalysts stability test was also performed. The experiment was carried out by a consecutive sweep from 0 to 1.2 V vs. RHE at 100 mV/s for 10,000 potential cycles in a 0.1 M $HClO_4$ solution. The curves stabilized after 10 cycles. The distribution of nanoparticles on Vulcan carbon support after 10,000 potential cycles is shown in Figs. S2(e)–S2(h) and S3(b) in the ESM. During the electrochemical treatment the NPs building the catalyst strongly aggregated.

In the case of the commercially available Pt catalyst, only few smaller, one bigger and some elongated agglomerates of Pt NPs on the carbon support are visible, some particles were detached probably due to carbon corrosion (Fig. S2(e) in the ESM). The structure of the Pt/Re/C (Fig. S2(g) in the ESM) and $Pt/SnO_2/C$ (Fig. S2(h) in the ESM) catalysts prepared in this work looks very similar after electrochemical experiments. Only for Pt/C, much smaller and uniformly distributed Pt NPs aggregates are visible. The nanoparticle distribution of the $Pt/Re/SnO_2/C$ catalyst is shown in Fig. S3(a) in the ESM for easier comparison with the catalyst structure after 10,000 potential cycles (Fig. S3(b) in the ESM). Potential cycling causes these nanoparticles to migrate in direction towards each other,

to form larger agglomerates which is visible in Fig. S3(b) in the ESM. For this catalyst detached nanoparticles were not observed in comparison to Pt TANAKA and Pt/SnO_2/C. The vanishing peak at about 0.45 and 0.75 V (Fig. 8(b)) probably indicates the loss of SnO_2. It could be related with degradation of tin above 1 V and after long electrochemical cycling [50]. Therefore, EDS measurements were performed to study the change of chemical composition of the nanoparticles before and after the electrochemical cycling. And in accordance to CV measurements, EDS confirmed lower tin content after electrochemical experiments (Table S1 in the ESM). It is also visible on FTIR spectra, in which the stretching vibrations of O–Sn–O coming from SnO_2 at 944 cm^{-1} wavenumber disappeared after 10,000 potential cycles (Fig. 4 and Table 1). In Fig. 8 additionally the decrease of ECSA for Pt TANAKA and Pt/Re/SnO_2/C is shown. Despite that the Pt TANAKA catalyst had an about three times larger electrochemical active surface compared to the ternary catalyst, it degraded faster. It can be seen from Fig. 8(a) that the H_2 desorption region for the commercial Pt TANAKA catalyst decreases rapidly (about 90%) in comparison to the Pt/Re/SnO_2/C catalyst, which after the accelerated stability test shows no significant variation. This observation indicates a better durability of Pt/Re/SnO_2/C catalyst compared to Pt TANAKA.

4 Discussion

In the present study the electrocatalytic activity towards EOR of catalysts consisting of one type, two or three types of nanoparticles was assessed. The binary and ternary combinations of the catalysts were successfully assembled via heteroaggregation [33, 35], which is confirmed by the STEM imaging combined with EDS mapping. However, TEM imaging did not show, if the synthesized nanoparticles are metallic or metal oxides. This information could also not be derived from the EDS spectra and maps, however the information about the chemical bonds between the atoms was assessed by FTIR spectroscopic measurements. In the IR range between 4,000 and 400 cm^{-1}, information about chemical bonds between metal surface and oxide can be derived. Thus, to verify that the synthesized nanoparticles are metallic or metal oxides, FTIR spectroscopy was used. If the Pt and Re nanoparticles underwent oxidation,

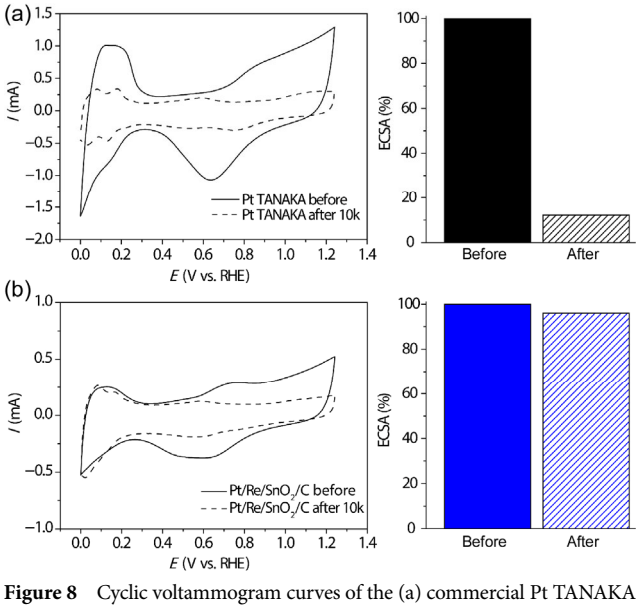

Figure 8 Cyclic voltammogram curves of the (a) commercial Pt TANAKA and (b) Pt/Re/SnO_2/C catalysts before and after 10,000 potential cycles with graphs showing the decrease of ECSA (%) (right column).

the vibrations of Pt–O and Re–O would be visible in the FTIR spectra at wavenumbers: 953 and 863 cm^{-1}, respectively [51, 52], which is not the case. This leads to the conclusion that the synthesized nanoparticles were metallic. Moreover, in the FTIR spectra of Pt/SnO_2/C and Pt/Re/SnO_2/C (Fig. 4 green and blue spectra, respectively), a vibration of OH from H_2O absorbed on the surface of SnO_2 or from decomposition of $HClO_4$ (1,619–1,635 cm^{-1}) was visible. Probably it originates from the decomposition of $HClO_4$, because as we concluded, SnO_2 degraded during electrochemical treatment, which was visible as decrease of the Sn signal in EDS and CV.

The electrochemical measurements revealed, that while the CVs curves for Pt TANAKA, Pt/C and Pt/Re/C showed a characteristic well-defined hydrogen adsorption–desorption region as usually observed for Pt catalyst, the cyclic voltammogram of the catalyst containing tin oxide (Pt/SnO_2/C and Pt/Re/SnO_2/C) additionally showed an increase in current density at the double layer, which could be related to the presence of Sn oxide species, and which is in good agreement with the literature reports [5, 46, 48, 49]. Li et al. indicated that this phenomena are usually assigned to the activation of H_2O on Sn and SnO_2 species on the platinum catalysts [48]. Peaks appearing around 0.45 and 0.7 V are attributed to the O_2 adsorption/desorption from the dissociation of water on Sn oxide and thus also could be related to the presence of tin oxide [46]. For ternary Pt/Re/SnO_2/C catalyst the current density at the double layer and peaks at about 0.45 and 0.7 V are higher even for Pt/SnO_2/C, which could be related to additional contribution of rhenium oxide. As XPS results showed in our previous work [33], the rhenium NPs were partly oxidized. It was also confirmed by XRD results (Fig. 3(b)). In the hydrogen absorption region, some differences also are visible. The hydrogen region for the catalysts synthesized in this work is modified in comparison to that region for commercially available platinum catalyst. This is due to the formation of oxygenated species on the Re or Sn atoms [53]. In the case of the Pt/Re/SnO_2/C catalyst, the hydrogen adsorption/desorption profile is characterized by large single peaks. The area of the hydrogen absorption region changes with the alteration in chemical composition of the catalyst. The larger area of the H_{ab} peak for the Pt/C catalyst than for the commercial Pt TANAKA, could be due to the smaller particle size of the Pt NPs and their better crystallinity as shown by the TEM observations (Figs. 1(a) and 2, and Fig. S6 in the ESM), influencing directly the ECSA value. The H_{ab} peaks for Pt/Re/C, Pt/SnO_2/C and Pt/Re/SnO_2/C are very similar to the one for the Pt/C catalyst. The difference that can be observed, is the result of the increase in current density at the double layer, which is associated with the presence of SnO_2. Moreover, the differences may be due to the variable number of adsorption sites for the hydrogen atoms. In Fig. 6(a), the catalytic activity towards ethanol oxidation reaction for nanocatalysts was compared. As clearly visible from the figure, by modifying and controlling the chemical composition of the nanocatalysts it is possible to enhance their catalytic properties.

The current values obtained for all synthesized nanocatalysts were always higher than those obtained for Pt TANAKA, which is in agreement with cyclic voltammetry experiments. The calculated ECSA is higher for the as-prepared Pt/C and Pt/Re/C than for other catalysts, probably due to the small size of platinum (around 2 nm) and rhenium nanoparticles (around 1 nm). Therefore, the current density for both synthesized catalysts could be higher in comparison to the commercial platinum catalyst, composed of larger (around 4.3 nm size) Pt nanoparticles (Fig. S6 in the ESM). In the case of the

Pt/SnO_2/C catalysts the addition of tin dioxide is clearly enhancing the ethanol electrooxidation reaction, which is consistent with many literature reports [45, 50, 54]. The current density is nearly fivefold higher than for commercial platinum (at 0.6 V vs. RHE). It was reported that the role of tin oxide is to promote the oxidation of CO_{ads} and facilitate its removal from the Pt surface, mitigating the effect of poisoning [55]. This effect is known as the bifunctional mechanism [56]: Sn provides OH species necessary for complete oxidation of ethanol to CO_2 [16]. Moreover, Lim et al. [46] deduced that, when SnO_2 nanoparticles are located in the vicinity of Pt nanoparticles, it is expected that SnO_2 will promote methanol and CO oxidations on the Pt sites. In the case of ethanol oxidation, the situation looks very similar and the overall catalytic activity is improved. It could be related to the ligand effect, where the presence of tin oxide close to platinum reduces the Pt–CO bond strength (bonding between the poisoning species and the catalyst surface) [16].

The ternary Pt/Re/SnO_2/C electrocatalyst showed the best catalytic activity for ethanol oxidation (Fig. 6(a))—more than 11 times and almost 8 times higher current density than commercial Pt at 0.45 and 0.6 V vs. RHE, respectively. Therefore, it can be concluded, that the addition of Re to the binary Pt/SnO_2/C catalysts definitely enhances its activity towards electro-oxidation of ethanol. As was mentioned, the synthesis of the Pt/Re/SnO_2/C catalysts was inspired by the system PtRh/SnO_2 studied in detail by Kowal et al. [22]. According to the literature, Rh is one of the rarest and most expensive precious metals; hence, to optimize and reduce the Rh content in the catalyst and eventually to replace Rh, is of great importance in designing applicable ethanol oxidation catalysts [20]. In this study, Re was used as an alternative to Rh in the ternary system to form a highly efficient EOR catalyst. According to the literature, the role of Rh is to enhance the catalytic reaction and cleave the C–C bond of ethanol, what was confirmed for example by density functional theory (DFT) calculations [22]. The information that Rh is responsible for the C–C bond cleavage was also underlined in other works [6, 20, 53, 57]. Rhenium has similar catalytic properties. Tayal et al. reported that rhenium is also known as a good catalyst for C–C bond breakage [24]. The role of rhenium has been investigated many times in the hydrogenation reactions of organic compounds [58], reforming [25, 26, 59] or recently as a catalyst component in the oxygen reduction reaction [60]. Re was found to be effective in breaking the C–C bond during reforming and cracking operations of petroleum fraction. So, the role of rhenium has previously been studied, but as one of the catalyst components for the oxidation of ethanol, it was probably first noticed and investigated by Basu et al. [24, 61]. However, the research subject of this group was rhenium as a component of a trimetallic alloy with platinum and tin. Nevertheless, the authors concluded that Re helps breaking the bond between C–C in the ethanol molecule. Despite that rhenium is also known as a strong binder of oxygen species, producing hydroxyl groups [26, 62], which also could facilitate removing the CO_{ads} produced due to C–C bond splitting. Moreover, literature reports indicate that the addition of Re to platinum catalysts weakens the binding energy between Pt and CO or other intermediate products, which not only increases the reaction rate at lower temperatures, but also leads to reducing the number of blocked catalytically active surface sites and consequently mitigates the poisoning of the catalyst [25, 26]. A too strong CO chemisorption increases CO site coverage and decreases the availability of operating catalytically active surface sites. Therefore, weaker adsorption strength could result in higher activity.

Additionally, it is worthwhile noticing, that in comparison to commercial Pt and other catalysts, for both nanocatalysts containing tin oxide (Pt//SnO_2/C and Pt/Re/SnO_2/C) the ethanol electro-oxidation is starting at much lower potentials (Figs. 6(e) and 6(f)). It is also a phenomenon visible in other works [24, 50, 61]. The negative potential shift can be attributed to the oxidation of the residues adsorbed on the catalyst surface by adsorbed OH species present on Sn oxide sites at lower potential than platinum [14, 63–65] and in case of the ternary Pt/Re/SnO_2/C catalyst, the effect is even greater due to the presence of rhenium, which may increase the percentage of the adsorbed OH species.

Chronoamperometry tests for the ethanol electrooxidation at 0.45 V vs. RHE also were carried out and the results are presented in Fig. 7(a). The drop of current densities of ethanol oxidation is definitely sharper for commercial platinum, Pt/C and Pt/Re/C catalysts than for the binary Pt/SnO_2/C and ternary Pt/Re/SnO_2/C catalyst. The curves for Pt/C and Pt/Re/C are practically overlapping. Nevertheless, as shown in Fig. 7(a), the currents for ethanol oxidation on all the catalysts dropped more or less rapidly and then became relatively stable. An initial increase in current was observed for all catalysts. As researchers suggested, it is probably related to the charging current or the catalyst poisoning during ethanol oxidation [24]. From the above observations, it can be concluded that the ternary catalyst shows the best stability and that the catalytic performance could be improved by addition of extra components to platinum. Moreover, the superior performance of Pt/Re/SnO_2/C electrocatalyst for ethanol oxidation could be attributed to the small 1 nm Re NPs and the synergistic effect between the elements: Pt, Re and SnO_2 (bifunctional mechanism and ligand effect). Certainly, the physical contact between the respective nanoparticles (Fig. 2) plays a crucial role, which was shown in our previous work [35], and has already been suggested by Kowal et al. [50], who indicated that the ethanol molecule has to be in contact with all phases of the catalyst in order to be completely oxidized. The situation looks similar in case of Pt/Re/SnO_2/C catalyst synthesized in this work. The synergistic effect is based on the "collaboration"—availability for the ethanol molecule of all three components, which are in direct contact with each other and each of them plays its own important role in the oxidation pathway. Thanks to the fact that rhenium is in the immediate vicinity of platinum, during catalysts (similarly as tin) it weakens the binding energy between the intermediate products of EOR and the surface of Pt (depoisoning the platinum surface). Crabb et al. [66] also noticed that the physical contact between SnO_2 and Pt particles would be an essential requirement for a synergistic effect between them. In Pt/Rh/SnO_2 obtained by Higuchi et al. [23], they also proved that the NPs are in partial contact. Inspired by this approach our research also has been focused on increasing the number of physical contact sites, because the presence of interfaces between the metal NPs and oxide (SnO_2) nanoparticles also could induce charge transfer, which could enhance the catalytic performance [67]. Therefore, larger (about 5 nm) SnO_2 NPs instead smaller, e.g. 2 nm were chosen/used in order to maximize the number of interface sites (Fig. 9). It allowed a more successful approach in preparing a catalyst with two or more components being in contact with each other. The most active sites in the Pt/Re/SnO_2/C catalyst are located at the interfaces between individual nanoparticles, precisely there, where the places of physical contact between Pt and SnO_2, Re and SnO_2 or Pt, Re and SnO_2 NPs are (which is indicated by black dashed arrows in scheme in Fig. 9 and is visible in the TEM image in Fig. 2(c)). It is also noticeable that

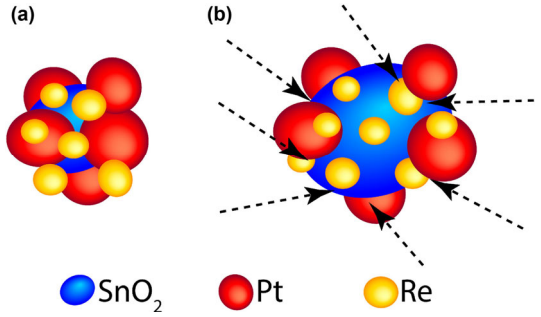

Figure 9 Schematic representation of (a) small 2 nm SnO_2 NPs and (b) larger 5 nm SnO_2 NPs surrounded by metallic Pt (red) and Re (orange) nanoparticles. Black dashed arrows indicate places of physical contact between individual NPs.

the ternary catalyst works better and shows higher current density despite that it has a nearly 3 times smaller electrochemical active surface than commercial Pt and more than 5 times compared to the Pt/C synthesized in this work (Table 2). It is due to the presence of tin oxide species, which are oxophilic and ensure easier removal of intermediates, such as CO, during the EOR [63]. Moreover, as shown in Figs. S2(b)–S2(d) and S3(a) in the ESM, all of the catalysts show uniform distribution. The surface chemistry of carbon is also a very important aspect. A uniform distribution of particles and their excellent attachment was achieved probably by the earlier functionalization of the carbon black (Vulcan XC-72R) with nitric acid (see Experimental section). In literature, researchers showed that it helps to create oxygenated groups on the surface [68, 69] and thus improve the catalytic activity towards the EOR and help attaching metal nanoparticles on the carbon support [70, 71].

Moreover, the obtained findings also show that the Pt/Re/SnO_2/C catalyst has a better durability compared to the commercial Pt TANAKA. According to the literature, the addition of Re and Sn to platinum catalysts weakens the binding energy of CO on Pt [25, 26] and hence CO poisoning is minimized [46]. So, the enhanced electrocatalytic durability of the Pt/Re/SnO_2/C catalysts for ethanol oxidation, similar to the highest current density in EOR, can be explained by the bifunctional effect and ligand effect in the electrocatalyst. As visible in the TEM images, showing the structure after the 10,000 potential cycles (Fig. S2 in the ESM), the catalysts degradation process is mainly attributed to agglomeration and detachment of NPs. It was also confirmed by ESCA calculations. As was shown in Fig. 8, the electrochemical treatment reduced the active surface area accessible for EOR. During the electrochemical treatments, the tin content also changed, which was confirmed by the vanishing peak at about 0.45 and 0.75 V on the CV curves (Fig. 8(b)) and EDS measurements (Table S1 in the ESM).

The new synthesis used in this study provides an easy and reproducible procedure for the preparation of ternary Pt/Re/SnO_2/C showing a predominant activity and durability compared to commercial Pt TANAKA, and could give a material being a good alternative as anode catalyst in low temperature fuel cell.

5 Conclusions

To summarize, catalysts consisting of platinum, rhenium and tin dioxide nanoparticles were structurally and chemically characterized and their electrocatalytic durability and activity towards EOR were investigated. The successful formation of binary and ternary combinations of the catalysts was confirmed by STEM and EDS analysis. The FTIR spectra acquired for the nanocatalysts served for their chemical analysis. The electrochemical activity towards ethanol oxidation was found to be better, when Re was present in the nanocatalysts. Despite the lowest electrochemical active surface area, the ternary Pt/Re/SnO_2/C catalyst showed the best catalytic activity towards EOR. The addition of Sn shifted the onset potential to more negative values, but the addition of rhenium intensified this effect and increased the shift even more. This is due to the synergistic effect between the three components of the studied ternary catalysts. Noticeable is also the fact, that Re helps to break the C–C bond of ethanol and prevents poisoning of the Pt surface. After 10,000 potential cycles of durability test, the ECSA decreased only slightly, demonstrating the high durability of ternary Pt/Re/SnO_2/C catalysts. Summarizing, the results in the present work showed that by choosing the appropriate metal composition and ensuring the physical contact between the nanoparticles forming the nanocatalysts, the overall catalytic activity towards the ethanol oxidation reaction and durability could be definitely improved.

Acknowledgments

The authors thank the Institute of Engineering Materials and Biomaterials of the Silesian University of Technology, for the use of the Titan FEI TEM instrument. Many thanks also to the Department of Chemistry, University of Warsaw for the access to the Talos F200 FEI TEM instrument. Dr. Ewa Juszyńska-Gałązka from Department of Soft Matter Research Institute of Nuclear Physics Polish Academy of Sciences is also acknowledged for her help in FTIR measurements. Many thanks to Dr. Alexey Maximenko for running the XRD measurements. Financial support from the Polish National Science Centre (NCN), grant UMO-2014/13/B/ST5/04497 is acknowledged.

Electronic Supplementary Material: Supplementary material (details of the ECSA calculations, TEM imaging and XRD measurements) is available in the online version of this article at https://doi.org/10.1007/s12274-020-2704-1.

References

[1] Jiang, K. Z.; Bu, L. Z.; Wang, P. T.; Guo, S. J.; Huang, X. Q. Trimetallic PtSnRh wavy nanowires as efficient nanoelectrocatalysts for alcohol electrooxidation. *ACS Appl. Mater. Interfaces* **2015**, *7*, 15061–15067.

[2] Erini, N.; Rudi, S.; Beermann, V.; Krause, P.; Yang, R. Z.; Huang, Y. H.; Strasser, P. Exceptional activity of a Pt-Rh-Ni ternary nanostructured catalyst for the electrochemical oxidation of ethanol. *ChemElectroChem* **2015**, *2*, 903–908.

[3] Yang, G. X.; Frenkel, A. I.; Su, D.; Teng, X. W. Enhanced electrokinetics of C–C bond splitting during ethanol oxidation by using a Pt/Rh/Sn catalyst with a partially oxidized Pt and Rh core and a SnO_2 shell. *ChemCatChem* **2016**, *8*, 2876–2880.

[4] Comignani, V.; Sieben, J. M.; Sanchez, M. D.; Duarte, M. M. E. Influence of carbon support properties on the electrocatalytic activity of PtRuCu nanoparticles for methanol and ethanol oxidation. *Int. J. Hydrogen Energy* **2017**, *42*, 24785–24796.

[5] Spinacé, E. V.; Linardi, M.; Neto, A. O. Co-catalytic effect of nickel in the electro-oxidation of ethanol on binary Pt-Sn electrocatalysts. *Electrochem. Commun.* **2005**, *7*, 365–369.

[6] Spinacé, E. V.; Dias, R. R.; Brandalise, M.; Linardi, M.; Neto, A. O. Electro-oxidation of ethanol using PtSnRh/C electrocatalysts prepared by an alcohol-reduction process. *Ionics* **2010**, *16*, 91–95.

[7] Yang, G. X.; Namin, L. M.; Aaron Deskins, N.; Teng, X. W. Influence of *OH adsorbates on the potentiodynamics of the CO_2 generation during the electro-oxidation of ethanol. *J. Catal.* **2017**, *353*, 335–348.

[8] Silva, J. C. M.; Parreira, L. S.; De Souza, R. F. B.; Calegaro, M. L.; Spinacé, E. V.; Neto, A. O.; Santos, M. C. PtSn/C alloyed and non-alloyed materials: Differences in the ethanol electro-oxidation reaction pathways. *Appl. Catal. B: Environ.* **2011**, *110*, 141–147.

[9] Antolini, E.; Colmati, F.; Gonzalez, E. R. Ethanol oxidation on carbon supported $(PtSn)_{alloy}/SnO_2$ and $(PtSnPd)_{alloy}/SnO_2$ catalysts with a fixed Pt/SnO_2 atomic ratio: Effect of the alloy phase characteristics. *J. Power Sources* **2009**, *193*, 555–561.

[10] Perez, J.; Paganin, V. A.; Antolini, E. Particle size effect for ethanol electro-oxidation on Pt/C catalysts in half-cell and in a single direct ethanol fuel cell. *J. Electroanal. Chem.* **2011**, *654*, 108–115.

[11] Zhou, W. P.; An, W.; Su, D.; Palomino, R.; Liu, P.; White, M. G.; Adzic, R. R. Electrooxidation of methanol at SnO_x-Pt interface: A tunable activity of tin oxide nanoparticles. *J. Phys. Chem. Lett.* **2012**, *3*, 3286–3290.

[12] Colmati, F.; Antolini, E.; Gonzalez, E. R. Preparation, structural characterization and activity for ethanol oxidation of carbon supported ternary Pt-Sn-Rh catalysts. *J. Alloys Compd.* **2008**, *456*, 264–270.

[13] Antolini, E.; Colmati, F.; Gonzalez, E. R. Effect of Ru addition on the structural characteristics and the electrochemical activity for ethanol oxidation of carbon supported Pt-Sn alloy catalysts. *Electrochem. Commun.* **2007**, *9*, 398–404.

[14] Jiang, L. H.; Sun, G. Q.; Sun, S. G.; Liu, J. G.; Tang, S. H.; Li, H. Q.; Zhou, B.; Xin, Q. Structure and chemical composition of supported Pt-Sn electrocatalysts for ethanol oxidation. *Electrochim. Acta* **2005**, *50*, 5384–5389.

[15] Antolini, E. Catalysts for direct ethanol fuel cells. *J. Power Sources* **2007**, *170*, 1–12.

[16] Antolini, E.; Gonzalez, E. R. Effect of synthesis method and structural characteristics of Pt-Sn fuel cell catalysts on the electro-oxidation of CH_3OH and CH_3CH_2OH in acid medium. *Catal. Today* **2011**, *160*, 28–38.

[17] Li, M.; Kowal, A.; Sasaki, K.; Marinkovic, N.; Su, D.; Korach, E.; Liu, P.; Adzic, R. R. Ethanol oxidation on the ternary Pt-Rh-SnO_2/C electrocatalysts with varied Pt:Rh:Sn ratios. *Electrochim. Acta* **2010**, *55*, 4331–4338.

[18] Du, W. X.; Yang, G. X.; Wong, E.; Deskins, N. A.; Frenkel, A. I.; Su, D.; Teng, X. W. Platinum-tin oxide core-shell catalysts for efficient electro-oxidation of ethanol. *J. Am. Chem. Soc.* **2014**, *136*, 10862–10865.

[19] Wang, C.; Jusys, Z.; Behm, R. J. Ethanol electro-oxidation on carbon-supported Pt, PtRu and Pt_3Sn catalysts: A quantitative DEMS study. *J. Power Sources* **2006**, *154*, 351–359.

[20] Li, M.; Cullen, D. A.; Sasaki, K.; Marinkovic, N. S.; More, K.; Adzic, R. R. Ternary electrocatalysts for oxidizing ethanol to carbon dioxide: Making Ir capable of splitting C–C bond. *J. Am. Chem. Soc.* **2013**, *135*, 132–141.

[21] Li, M.; Zhou, W. P.; Marinkovic, N. S.; Sasaki, K.; Adzic, R. R. The role of rhodium and tin oxide in the platinum-based electrocatalysts for ethanol oxidation to CO_2. *Electrochim. Acta* **2013**, *104*, 454–461.

[22] Kowal, A.; Li, M.; Shao, M.; Sasaki, K.; Vukmirovic, M. B.; Zhang, J.; Marinkovic, N. S.; Liu, P.; Frenkel, A. I.; Adzic, R. R. Ternary $Pt/Rh/SnO_2$ electrocatalysts for oxidizing ethanol to CO_2. *Nat. Mater.* **2009**, *8*, 325–330.

[23] Higuchi, E.; Takase, T.; Chiku, M.; Inoue, H. Preparation of ternary $Pt/Rh/SnO_2$ anode catalysts for use in direct ethanol fuel cells and their electrocatalytic activity for ethanol oxidation reaction. *J. Power Sources* **2014**, *263*, 280–287.

[24] Tayal, J.; Rawat, B.; Basu, S. Effect of addition of rhenium to Pt-based anode catalysts in electro-oxidation of ethanol in direct ethanol PEM fuel cell. *Int. J. Hydrogen Energy* **2012**, *37*, 4597–4605.

[25] Simonetti, D. A.; Kunkes, E. L.; Dumesic, J. A. Gas-phase conversion of glycerol to synthesis gas over carbon-supported platinum and platinum-rhenium catalysts. *J. Catal.* **2007**, *247*, 298–306.

[26] Ciftci, A.; Ligthart, D. A. J. M.; Sen, A. O.; Van Hoof, A. J. F.; Friedrich, H.; Hensen, E. J. M. Pt-Re synergy in aqueous-phase reforming of glycerol and the water-gas shift reaction. *J. Catal.* **2014**, *311*, 88–101.

[27] Ramstad, A.; Strisland, F.; Raaen, S.; Borg, A.; Berg, C. CO and O_2 adsorption on the Re/Pt(111) surface studied by photoemission and thermal desorption. *Surf. Sci.* **1999**, *440*, 290–300.

[28] Duke, A. S.; Xie, K. M.; Monnier, J. R.; Chen, D. A. Superior long-term activity for a Pt-Re alloy compared to Pt in methanol oxidation reactions. *Surf. Sci.* **2017**, *657*, 35–43.

[29] Infoplease: *Math & Science, Chemistry, Interactive Periodic Table* [Online]. https://www.infoplease.com/transition-metals/rhenium & https://www.infoplease.com/transition-metals/platinum (accessed Feb 20, 2020).

[30] Erini, N.; Loukrakpam, R.; Petkov, V.; Baranova, E. A.; Yang, R. Z.; Teschner, D.; Huang, Y. H.; Brankovic, S. R.; Strasser, P. Ethanol electro-oxidation on ternary platinum-rhodium-tin nanocatalysts: Insights in the atomic 3D structure of the active catalytic phase. *ACS Catal.* **2014**, *4*, 1859–1867.

[31] Alnot, M.; Gorodetskii, V.; Cassuto, A.; Ehrhardt, J. J. Auger electron spectroscopy, X-ray photoelectron spectroscopy, work function measurements and photoemission of adsorbed xenon on thin films of Pt-Re(111) alloys. *Thin Solid Films* **1987**, *151*, 251–262.

[32] Duke, A. S.; Galhenage, R. P.; Tenney, S. A.; Sutter, P.; Chen, D. A. *In situ* studies of carbon monoxide oxidation on platinum and platinum-rhenium alloy surfaces. *J. Phys. Chem. C* **2015**, *119*, 381–391.

[33] Drzymała, E.; Gruzeł, G.; Pajor-Świerzy, A.; Depciuch, J.; Socha, R.; Kowal, A.; Warszyński, P.; Parlinska-Wojtan, M. Design and assembly of ternary $Pt/Re/SnO_2$ NPs by controlling the zeta potential of individual Pt, Re, and SnO_2 NPs. *J. Nanopart. Res.* **2018**, *20*, 144.

[34] Roth, C.; Papworth, A. J.; Hussain, I.; Nichols, R. J.; Schiffrin, D. J. A Pt/Ru nanoparticulate system to study the bifunctional mechanism of electrocatalysis. *J. Electroanal. Chem.* **2005**, *581*, 79–85.

[35] Parlinska-Wojtan, M.; Drzymała, E.; Gruzeł, G.; Depciuch, J.; Donten, M.; Kowal, A. Ternary $Pt/Re/SnO_2$ nanoparticles for ethanol oxidation reaction: Understanding the correlation between the synthesis route and the obtained material. *Appl. Catal. A: Gen.* **2019**, *570*, 319–328.

[36] De Souza, E. A.; Giz, M. J.; Camara, G. A.; Antolini, E.; Passos, R. R. Ethanol electro-oxidation on partially alloyed Pt-Sn-Rh/C catalysts. *Electrochim. Acta* **2014**, *147*, 483–489.

[37] Sivaiah, K.; B. Hemalatha Rudramadevi, B.; Buddhudu, S.; Bhaskar Kumar, G.; Varadarajulu, A. Structural, thermal and optical properties of Cu^{2+} and Co^{2+}: PVP polymer films. *Indian J. Pure Appl. Phys.* **2010**, *48*, 658–662.

[38] Krishnan, K.; Krishnan, R. S. Raman and infrared spectra of ethylene glycol. *Proc. Indian Acad. Sci. - Sect. A* **1966**, *64*, 111.

[39] Plyler, E. K. Infrared spectra of methanol, ethanol, and n-propanol. *J. Res. Natl. Bur. Stand.* **1952**, *48*, 281–286.

[40] Mariammal, R. N.; Rajamanickam, N.; Ramachandran, K. Synthesis and characterization of undoped and Co-doped SnO_2 nanoparticles. *J. Nano-Electron. Phys.* **2011**, *3*, 92–100.

[41] Chen, D. L.; Gao, L. A. Novel synthesis of well-dispersed crystalline SnO_2 nanoparticles by water-in-oil microemulsion-assisted hydrothermal process. *J. Colloid Interface Sci.* **2004**, *279*, 137–142.

[42] Krishnakumar, T.; Pinna, N.; Kumari, K. P.; Perumal, K.; Jayaprakash, R. Microwave-assisted synthesis and characterization of tin oxide nanoparticles. *Mater. Lett.* **2008**, *62*, 3437–3440.

[43] Solymosi, F.; Block, J. H. Catalytic decomposition of $HClO_4$ vapor over CuO by field ion mass spectrometry. *J. Catal.* **1976**, *42*, 173–176.

[44] Karelin, A. I.; Grigorovich, Z. I. Vibrational spectra of perchloric acid—II. Modifications and phase transitions of solid $HClO_4$ and $DClO_4$. *Spectrochim. Acta Part A: Mol. Spectrosc.* **1976**, *32*, 851–857.

[45] Dou, M. L.; Hou, M.; Liang, D.; Lu, W. T.; Shao, Z. G.; Yi, B. L. SnO_2 nanocluster supported Pt catalyst with high stability for proton exchange membrane fuel cells. *Electrochim. Acta* **2013**, *92*, 468–473.

[46] Lim, D. H.; Choi, D. H.; Lee, W. D.; Lee, H. I. A new synthesis of a highly dispersed and CO tolerant PtSn/C electrocatalyst for low-temperature fuel cell; its electrocatalytic activity and long-term durability. *Appl*. *Catal*. *B*: *Environ*. **2009**, *89*, 484–493.
[47] Binninger, T.; Fabbri, E.; Kötz, R.; Schmidt, T. J. Determination of the electrochemically active surface area of metal-oxide supported platinum catalyst. *J*. *Electrochem*. *Soc*. **2014**, *161*, H121–H128.
[48] Li, H. Q.; Sun, G. Q.; Cao, L.; Jiang, L. H.; Xin, Q. Comparison of different promotion effect of PtRu/C and PtSn/C electrocatalysts for ethanol electro-oxidation. *Electrochim*. *Acta* **2007**, *52*, 6622–6629.
[49] De Lima, R. B.; Paganin, V.; Iwasita, T.; Vielstich, W. On the electrocatalysis of ethylene glycol oxidation. *Electrochim*. *Acta* **2003**, *49*, 85–91.
[50] Kowal, A.; Gojković, S. L.; Lee, K. S.; Olszewski, P.; Sung, Y. E. Synthesis, characterization and electrocatalytic activity for ethanol oxidation of carbon supported Pt, Pt-Rh, Pt-SnO_2 and Pt-Rh-SnO_2 nanoclusters. *Electrochem*. *Commun*. **2009**, *11*, 724–727.
[51] Luo, J. H.; Alexander, B.; Wagner, T. R.; Maggard, P. A. Synthesis and characterization of ReO_4-containing microporous and open framework structures. *Inorg*. *Chem*. **2004**, *43*, 5537–5542.
[52] Gong, Y.; Zhou, M. F. Infrared spectra of transition-metal dioxide anions: MO_2^- (M = Rh, Ir, Pt, Au) in solid argon. *J*. *Phys*. *Chem*. *A* **2009**, *113*, 4990–4995.
[53] Lima, F. H. B.; Gonzalez, E. R. Ethanol electro-oxidation on carbon-supported Pt-Ru, Pt-Rh and Pt-Ru-Rh nanoparticles. *Electrochim*. *Acta* **2008**, *53*, 2963–2971.
[54] Jiang, L.; Colmenares, L.; Jusys, Z.; Sun, G. Q.; Behm, R. J. Ethanol electrooxidation on novel carbon supported Pt/SnO_x/C catalysts with varied Pt:Sn ratio. *Electrochim*. *Acta* **2007**, *53*, 377–389.
[55] St. John, S.; Boolchand, P.; Angelopoulos, A. P. Improved electrocatalytic ethanol oxidation activity in acidic and alkaline electrolytes using size-controlled Pt-Sn nanoparticles. *Langmuir* **2013**, *29*, 16150–16159.
[56] Vigier, F.; Coutanceau, C.; Hahn, F.; Belgsir, E. M.; Lamy, C. On the mechanism of ethanol electro-oxidation on Pt and PtSn catalysts: Electrochemical and *in situ* IR reflectance spectroscopy studies. *J*. *Electroanal*. *Chem*. **2004**, *563*, 81–89.
[57] Mai, P. T.; Haze, A.; Chiku, M.; Higuchi, E.; Inoue, H. Ethanol oxidation reaction on tandem Pt/Rh/SnO_x catalyst. *Catalysts* **2017**, *7*, 246.
[58] Davenport, W. H.; Kollonitsch, V.; Klein, C. H. Advances in rhenium catalysts. *Ind*. *Eng*. *Chem*. **1968**, *60*, 10–19.
[59] Kirilin, A. V.; Tokarev, A. V.; Manyar, H.; Hardacre, C.; Salmi, T.; Mikkola, J. P.; Murzin, D. Y. Aqueous phase reforming of xylitol over Pt-Re bimetallic catalyst: Effect of the Re addition. *Catal*. *Today* **2014**, *223*, 97–107.
[60] Raciti, D.; Kubal, J.; Ma, C.; Barclay, M.; Gonzalez, M.; Chi, M. F.; Greeley, J.; More, K. L.; Wang, C. Pt_3Re alloy nanoparticles as electrocatalysts for the oxygen reduction reaction. *Nano Energy* **2016**, *20*, 202–211.
[61] Goel, J.; Basu, S. Pt-Re-Sn as metal catalysts for electro-oxidation of ethanol in direct ethanol fuel cell. *Energy Procedia* **2012**, *28*, 66–77.
[62] Zhang, L.; Karim, A. M.; Engelhard, M. H.; Wei, Z. H.; King, D. L.; Wang, Y. Correlation of Pt-Re surface properties with reaction pathways for the aqueous-phase reforming of glycerol. *J*. *Catal*. **2012**, *287*, 37–43.
[63] Gharibi, H.; Sadeghi, S.; Golmohammadi, F. Electrooxidation of Ethanol on highly active and stable carbon supported $PtSnO_2$ and its application in passive direct ethanol fuel cell: Effect of tin oxide synthesis method. *Electrochim*. *Acta* **2016**, *190*, 1100–1112.
[64] Colmati, F.; Antolini, E.; Gonzalez, E. R. Effect of temperature on the mechanism of ethanol oxidation on carbon supported Pt, PtRu and Pt_3Sn electrocatalysts. *J*. *Power Sources* **2006**, *157*, 98–103.
[65] Colmati, F.; Antolini, E.; Gonzalez, E. R. Pt–Sn/C electrocatalysts for methanol oxidation synthesized by reduction with formic acid. *Electrochim*. *Acta* **2005**, *50*, 5496–5503.
[66] Crabb, E. M.; Marshall, R.; Thompsett, D. Carbon monoxide electro-oxidation properties of carbon-supported PtSn catalysts prepared using surface organometallic chemistry. *J*. *Electrochem*. *Soc*. **2000**, *147*, 4440–4447.
[67] An, K.; Somorjai, G. A. Nanocatalysis I: Synthesis of metal and bimetallic nanoparticles and porous oxides and their catalytic reaction studies. *Catal*. *Lett*. **2015**, *145*, 233–248.
[68] Calvillo, L.; Celorrio, V.; Moliner, R.; Lázaro, M. J. Influence of the support on the physicochemical properties of Pt electrocatalysts: Comparison of catalysts supported on different carbon materials. *Mater*. *Chem*. *Phys*. **2011**, *127*, 335–341.
[69] Rizo, R.; Sebastián, D.; Lázaro, M. J.; Pastor, E. On the design of Pt-Sn efficient catalyst for carbon monoxide and ethanol oxidation in acid and alkaline media. *Appl*. *Catal*. *B*: *Environ*. **2017**, *200*, 246–254.
[70] Alegre, C.; Gálvez, M. E.; Baquedano, E.; Pastor, E.; Moliner, R.; Lázaro, M. J. Influence of support's oxygen functionalization on the activity of Pt/carbon xerogels catalysts for methanol electro-oxidation. *Int*. *J*. *Hydrogen Energy* **2012**, *37*, 7180–7191.
[71] Sebastián, D.; Suelves, I.; Moliner, R.; Lázaro, M. J. The effect of the functionalization of carbon nanofibers on their electronic conductivity. *Carbon* **2010**, *48*, 4421–4431.